Materials Science & Engineering A 893 (2024) 146140

Contents lists available at ScienceDirect

Materials Science & Engineering A

journal homepage: www.elsevier.com/locate/msea

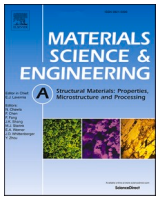

Influence of Cr and Cr+Nb on the interphase precipitation and mechanical properties of V–Mo microalloyed steels

Karol F. Rodriguez-Galeano [a,b], John Nutter [a], Yunus Azakli [a], Carl Slater [c], W. Mark Rainforth [a,*]

[a] Department of Materials Science and Engineering, The University of Sheffield, Sir Robert Hadfield Building, Mappin Street, Sheffield, S1 3JD, UK
[b] TATA Steel, 1970, CA, Ijmuiden, the Netherlands
[c] Advanced Steel Research Centre, University of Warwick, Coventry, CV4 7AL, UK

A B S T R A C T

There has been much research on steels strengthened by interphase precipitation, but the role of Cr remains unclear. Isothermal transformations have been performed at different temperatures to investigate the effect of Cr and Cr + Nb additions on the interphase precipitation resulting from the austenite-to-ferrite transformations in V–Mo based dual phase steels. Optical microscopy (OM) plus transmission electron microscopy (TEM) and tensile testing were used to characterize and correlate microstructural evolution to the tensile properties and the interphase precipitation formed during the austenite to ferrite ($\gamma \rightarrow \alpha$) transformation. It was found that an addition of 0.5 wt% Cr to V–Mo microalloyed steel accelerates the transformation rate of ferrite, producing a higher volume fraction of ferrite. Importantly, the addition of Cr reduces the diameter of the interphase precipitates giving an important contribution to the yield strength. A further addition of 0.03 wt% Nb to the Cr–V–Mo reduces the contribution made by the interphase precipitation and increased the grain refined contribution. A new method was used to calculate the volume fraction of interphase precipitation with TEM images from extraction replicas is presented and included in a root-mean-square model which includes the precipitation hardening made by IP on microalloyed DP steels to effectively predict their yield strength.

1. Introduction

Developed from conventional low-allow steels, dual-phase (DP) steels consisting of ferrite plus martensite present an attractive combination of tensile properties, like good relation strength-formability with continuous yielding, high work hardening rate, and low yield ratio [1]. Traditionally, the strengthening of DP steels through modification of the chemistry involves one of the two possible routes: to increase the carbon content, but this strongly hinders the weldability, or adding alloying elements, but this increases the material cost. Alloy additions such as Mn, Mo, Nb, Ta, Cr and B lead to an increased tensile strength due to the grain refining effect of these elements, but with no improvement in the hole-expansion behaviour [2,3]. It has long been known that appropriate thermomechanical processing can produce high-strength low--alloy ferritic steels with good formability at low production cost [4,5]. The nano-sized alloy carbides formed within the ferrite increase the yield strength. These carbides can precipitate in any of three ways: in supersaturated austenite, on the austenite/ferrite interface during transformation, or in supersaturated ferrite. Precipitation formed during the austenite/ferrite interface are called interphase precipitation and are known for forming in a periodic row dispersion of nano-sized carbides which give an important contribution to the yield and ultimate tensile strength. Other studies were focused in the study of the effect of carbide-forming elements additions such as V, Mo, Nb, Cr, Ti, and W to DP low-alloy steels, demonstrating that these elements cannot diffuse as fast as carbon in iron and promoting the formation of interphase precipitation [6–10], some increasing the transformation kinetics (Ti, V, and Nb), and others slowing it down (Cr, Mo and W) [11].

There has been very extensive research on interphase precipitation with particular attention paid to the nature of the interface between austenite and ferrite [6,12–16]. It is well established that interphase precipitation is controlled by four factors (in no particular order), namely a) the interface mobility, b) solute drag, c) the phase equilibria at the interface, and d) the orientation relationship (OR) between the austenite and the ferrite. While there is now a strong theoretical understanding of the transforming interface, the practical role of some alloy additions remains unclear, in particular, the role of small Cr additions to Fe–*C*–V interphase precipitation system is unclear. There is no interphase precipitation with Cr as the main carbide/carbonitride forming alloy addition, but Cr does affect the solubility of other microalloying additions such as Ti [17,18], and Nb [18–20], and, of course, Cr promotes austenite to ferrite transformation [21].

To understand the effect of Cr on the interphase precipitation of microalloyed steels as a contributor to their tensile properties, three

* Corresponding author.
E-mail address: m.rainforth@sheffield.ac.uk (W.M. Rainforth).

https://doi.org/10.1016/j.msea.2024.146140
Received 16 October 2023; Received in revised form 14 December 2023; Accepted 16 January 2024
Available online 17 January 2024

alloys were prepared with the same base composition (V–Mo). One steel has no Cr, another is based on a Cr microalloy addition, and the third with the combined effect of Cr and a strong grain refiner and carbide former element, Nb. Interphase precipitation was induced by isothermal transformation at different temperatures following a rapid cool from the austenitisation temperature. A meticulous analysis of the interphase precipitates has been undertaken, characterizing their composition, volume fraction, and size to correlate and understand the role of Cr and Cr + Nb on the mechanical properties of these microalloyed DP steels.

2. Experimental procedure

2.1. Materials

Three microalloyed steels with different Cr and Cr + Nb contents were studied. Table 1 lists the chemical compositions of the alloys with the notation used to describe each alloy. All steels were made by vacuum induction melting, cast into 80 mm × 80 mm × 100 mm blocks at the University of Sheffield, then divided into two blocks 80 mm × 80 mm × 40 mm and homogenized at 1250 °C for 2 h. The hot rolling schedule is shown in Table 2, with a starting rolling temperature of 1000 °C and a final rolling temperature of 975 °C.

Dilatometer specimens were machined from the rolled plate along the rolling directions with dimensions of 150 mm long × 15 mm wide × the thickness of the plate. To produce the interphase precipitation, samples were reheated to 1250 °C and held for 30 min in a tube furnace and further water quenched to control the prior-austenite grain size before the isothermal transformation. A Dilatronic dilatometer at the University of Sheffield was used for the isothermal transformation. Dilatometer samples were reaustenitized at 1200 °C for 3 min and cooled to the desired isothermal transformation temperature (T_{iso}) at a rate of 10 °C/s^{-1}, held isothermally for 1.5 h and finally water quenched to room temperature. The reheating and reaustenitization of the Cr–Nb–V–Mo steel was undertaken at 1100 °C to prevent the dissolution of Nb precipitates and to limit grain growth [22]. The isothermal transformation was performed at temperatures in the range 600–710 °C to investigate the effect of transformation temperature on the nature of interphase precipitation and the ferrite volume fraction. The full scheme of the heat treatment schedule is shown in Fig. 1. Each treatment was repeated three times and the results presented are the average of them.

2.2. Prior-austenite grain size, ferrite volume fraction, ferrite grain size and tensile properties

Samples of 20 mm × 20 mm × plate thickness (11 mm) where cut from the hot-rolled sheet and reheated to 1250 °C (steels V–Mo and Cr–V–Mo) and to 1100 °C (steel Nb–Cr–V–Mo) for 30 min, then cut in half, prepared using standard methods for microstructural analysis and etched with a 2 % picral etchant [23] to reveal and measure the prior-austenite grains. The intercept linear method (ASTM E−112) via Image J software was used to measure the prior-austenite grain size.

Samples for both tensile testing and metallography were removed from the dilatometer samples. In each case, samples were removed close to where the thermocouple was located in order to ensure the thermal history was known. Metallographic samples were prepared using standard techniques and etched in a 2 % nital solution. The volume fraction of ferrite was determined by the point counting method. The intercept linear method (ASTM E−112) via Image J software measured the ferrite grain size in the corresponding optical samples. Tensile samples of the three alloys were manufactured after the metallographic examination to guarantee the structure of the testing sample was homogeneous along the gauge section. Samples for tensile test of all alloys were manufactured along the rolling direction, following the recommended dimensional relationship suggested by the GB standard $L_0/\sqrt{A_0} = 5$, with a gauge section of 2 × 2.4 × 11 mm which gives a more conservative result of the total elongation than the recommended by the ASTM E8M.

Table 2
Hot-rolling initial and final thickness per pass for steels Cr–Nb–V–Mo.

Pass	Initial thickness [mm]	Final thickness [mm]
1st	40.0	34.2
2nd	34.2	28.4
3rd	28.4	22.6
4th	22.6	16.8
5th	16.8	11.0

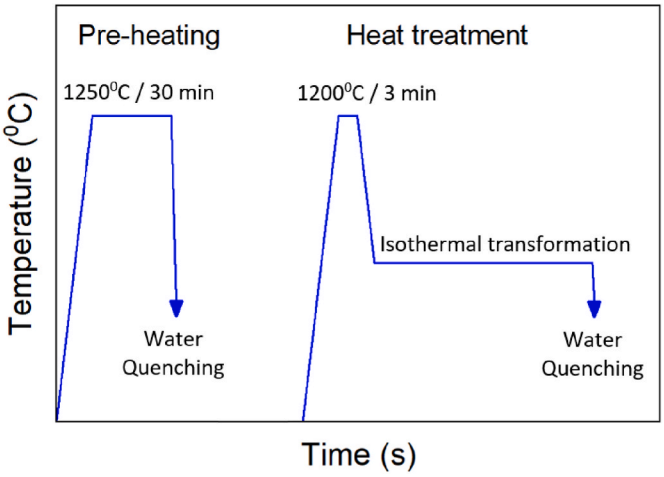

Fig. 1. Scheme of the general heat treatment to produce interphase precipitation.

2.3. Precipitate analysis

For characterization and measurement of the interphase precipitation, transmission electron microscopy (TEM) was carried out. Carbon extraction replicas were used to measure the precipitate size and volume fraction. Gong et al. [10] showed that precipitate size and distribution obtained from carbon extraction replicas are the same as from STEM images from thin foil samples within experimental error. Thin foil samples were produced by cutting the slices from the optical examination specimens, thinning them mechanically to 100 μm by abrasion and then electropolished using an electrolyte solution of 60 % methanol, 35 % butoxyethanol and 5 % perchloric acid. The carbon extraction replicas were prepared in the standard manner, using a 2 % nital solution for the light etching, then the carbon depositions were made with a Quorum Q150T ES plus coater (around 7 nm). For the extraction and collection of the replicas, a 10 % nital etchant was used. Both, extraction replica and thin foil samples were examined using a JEOL JEM F200 operating at 200 kV. The particle diameter and fraction of interphase precipitation

Table 1
Chemical composition of the alloys V–Mo, Cr–V–Mo and Cr–Nb–V–Mo.

	C	Mn	Si	Al	V	Mo	Cr	N	Nb
V–Mo	0.12	1.41	0.21	<0.005	0.2	0.48	–	<0.003	–
Cr–V–Mo	0.13	1.56	0.19	<0.005	0.21	0.5	0.51	<0.003	–
Cr–Nb–V–Mo	0.13	1.42	0.25	0.016	0.21	0.51	0.48	<0.003	0.03

were measured for each sample, counting a minimum of 5000 particles per sample with the particle counter function of the software Image J.

3. Results

3.1. Prior-austenite grain size

The prior austenite structure was observed via optical micrographs from the 20 mm × 20 mm × plate thickness (11 mm) specimens cut from the hot-rolled plate, after a reheating for 30 min. Fig. 2 shows the austenite grain boundaries for the three steels, with average values of 42 μm, 41.3 μm, and 13.6 μm measured for the V–Mo, Cr–V–Mo, and Cr–Nb–V–Mo steels respectively.

3.2. Microstructure

For the microstructure observation, all optical micrographs were taken from the dilatometer samples isothermally treated at different temperatures for 90 min. Fig. 3 - Fig. 5 show the microstructure of steels V–Mo, Cr–V–Mo, and Cr–Nb–V–Mo. As expected, the microstructure comprises allotriomorphic ferrite (light contrast) and martensite (dark contrast), with the latter originating during the final quench due transformation of the untransformed austenite. Fig. 3 shows the V–Mo steel for various transformation temperatures, showing that the ferrite is largely polygonal across all isothermal transformation temperatures, although a small amount of displacive transformation products (e.g., acicular ferrite) is also present. Above 655 °C, the higher the temperature of the isothermal transformation, the lower the ferrite fraction and the stronger the banding effect.

Fig. 4 shows the microstructures obtained in the Cr–V–Mo steel for transformation between 645 °C and 675 °C, which is mainly comprised of polygonal ferrite, with some Widmanstätten [18] ferrite and martensite. Fig. 5 shows optical micrographs of the Cr–Nb–V–Mo steel. It is clear that the addition of Cr + Nb to the V–Mo microalloyed steel moves the TTT curve upward, also reducing the temperature range in which the γ→α transformation occurs, which is a reflection of the smaller austenite grain size in this steel [24]. Isothermal transformation at 640 °C produces bainite with some very fine zones of incompletely transformed ferrite. The fraction of bainite reduces while the temperature of isothermal transformation increases. At 700 °C massive blocks of ferrite are produced along with lath martensite.

The ferrite volume fraction and the ferrite grain size (polygonal ferrite only) of the three microalloyed steels are presented in Fig. 6. The volume fraction of polygonal ferrite in the Cr-free microalloy steel was lower than in the microalloyed steel with Cr for isothermal transformations between 655 and 670 °C. The fraction of total ferrite increases for the V–Mo from 600 °C to a maximum at ~655 °C and then falls again at higher temperatures. The Cr–V–Mo steel showed similar behaviour, but the maximum ferrite content was ~17 % higher than the V–Mo and the peak in ferrite content occurred at 665 °C, Fig. 5a. In contrast, for the Cr–V–Mo–Nb steel, the ferrite fraction increases from 675 to 700 °C, where it reaches a maximum and then falls again at higher temperatures. The maximum ferrite fraction for this steel was the lowest of all at ~60 %.

There is little difference in the polygonal ferrite grain size between the V–Mo steel and the Cr–V–Mo steel, Fig. 5b, and both show little variation with transformation temperature. The Cr–Nb–V–Mo steel again shows quite different behaviour to the other two steels, with a smaller polygonal ferrite grain size, which is expected from the Nb additions [25–27], but the change with temperature is more complicated with a minimum found at 675 °C, increasing up to 680 °C and then approximately constant values above 683 °C. Of course, the grain size range was variable between the steels (as shown by the error bar size). Examples of this are shown in Fig. 5 b) and d) where some finer polygonal ferrite grains can be seen in certain regions.

3.3. Kinetics of phase transformation

Fig. 7 shows the dilatation curves of the three alloys isothermally transformed at several temperatures for 90 min. A simple conclusion on the effect of Cr addition on the rate of transformation cannot be drawn. At 640 °C the Cr addition reduces the time for the $\gamma \rightarrow \alpha$ phase transformation and changes the allotriomorphic ferrite structure in the Cr-free steel to a polygonal shaped ferrite in the steel with Cr additions.

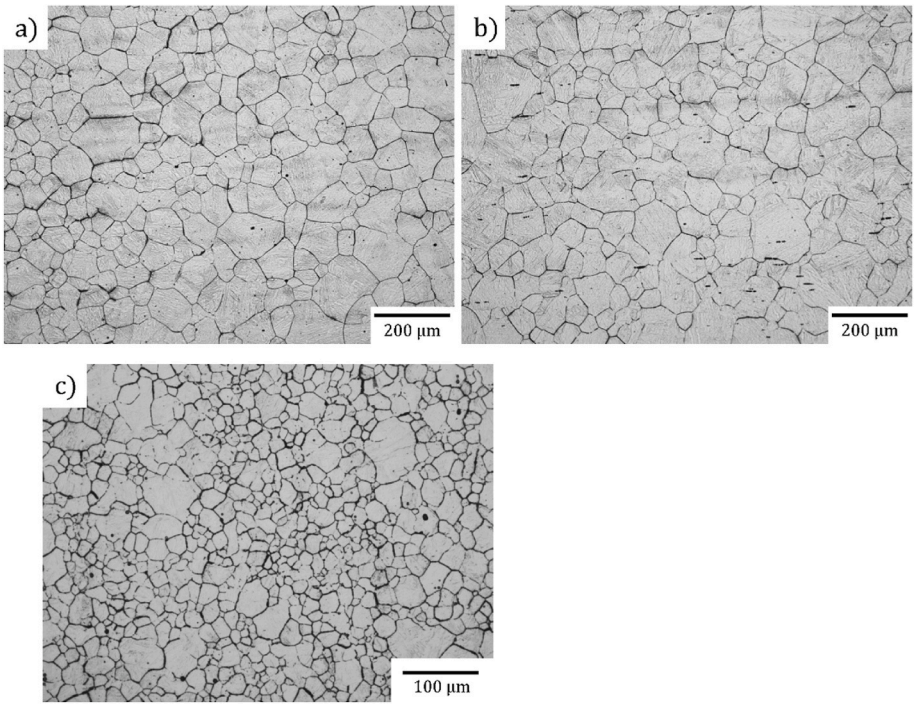

Fig. 2. Prior austenite grains of a) V–Mo steel reheated to 1250 °C, b) Cr–V–Mo steel reheated to 1250 °C, and a) Nb–Cr–V–Mo steel reheated to 1100 °C.

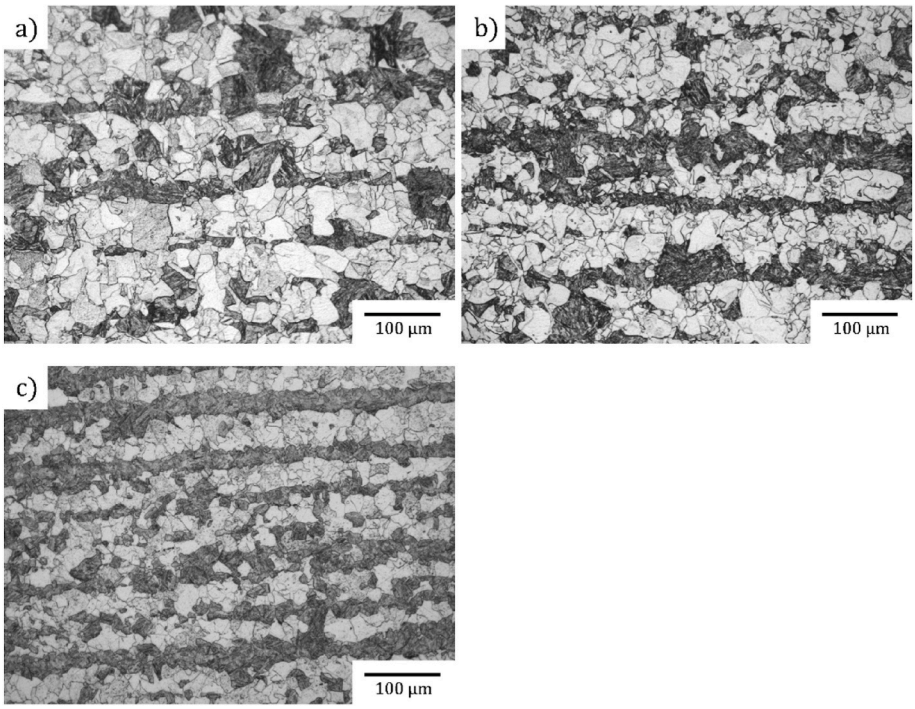

Fig. 3. V–Mo steel Isothermally transformed a) 640 °C, b) 655 °C, c) 670 °C.

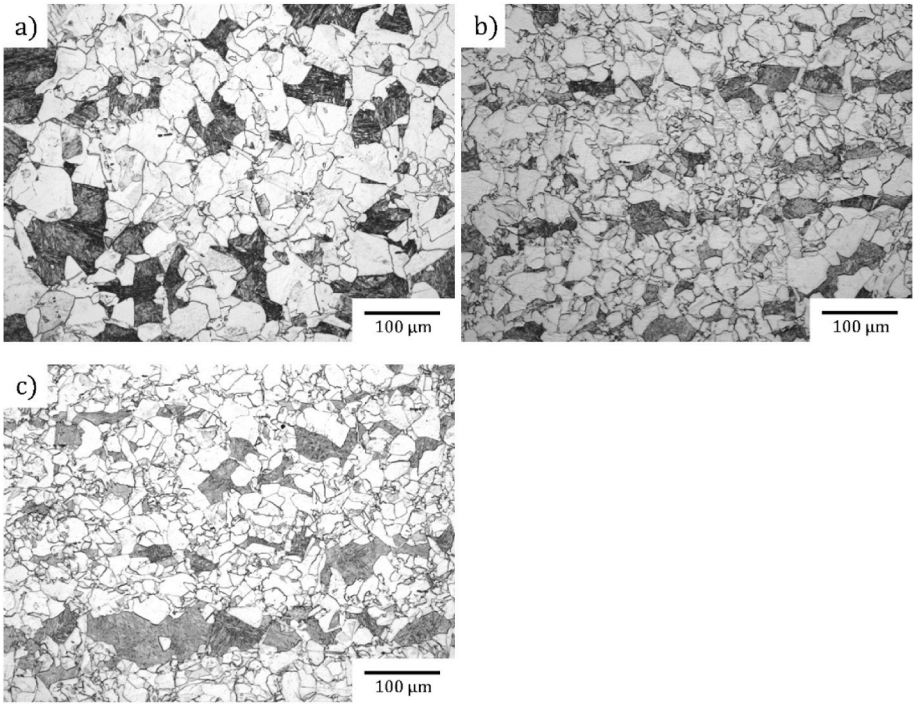

Fig. 4. Cr–V–Mo steel Isothermally transformed a) 650 °C, b) 665 °C, c) 670 °C.

For isothermal transformation at 670 °C the transformation rate appears similar in the dilatometer data. However, the volume fraction of ferrite is significantly higher (~15 %, Fig. 6a) in the Cr–V–Mo steel compared to the V–Mo steel, and therefore the transformation rate was higher in the Cr–V–Mo steel.

The combined addition of Cr and Nb to the V–Mo microalloyed steels led to shorter transformation times than Cr-free and Cr-added V–Mo microalloyed steels. Moreover, this addition produced the opposite effect to that of Cr on its own, by increasing the temperatures where $\gamma \rightarrow \alpha$ transformation occurs and extending the required time for transformation.

3.4. Transmission electron microscopy

The precipitate morphology was investigated both by thin foil TEM and extraction replicas. All the diffraction patterns were taken from thin foil samples. Figs. 8 and 9 show TEM micrographs of the interphase precipitation in the V–Mo and Cr–V–Mo steels. VC precipitates were

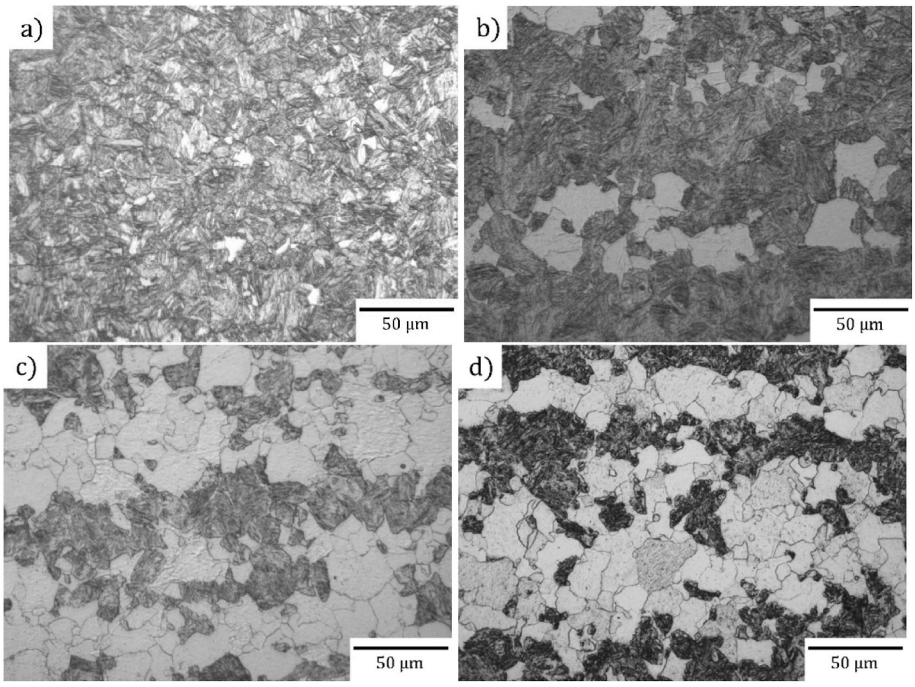

Fig. 5. Cr–Nb–V–Mo steel Isothermally transformed a) 665 °C, b) 680 °C, c) 700 °C, d) 710 °C.

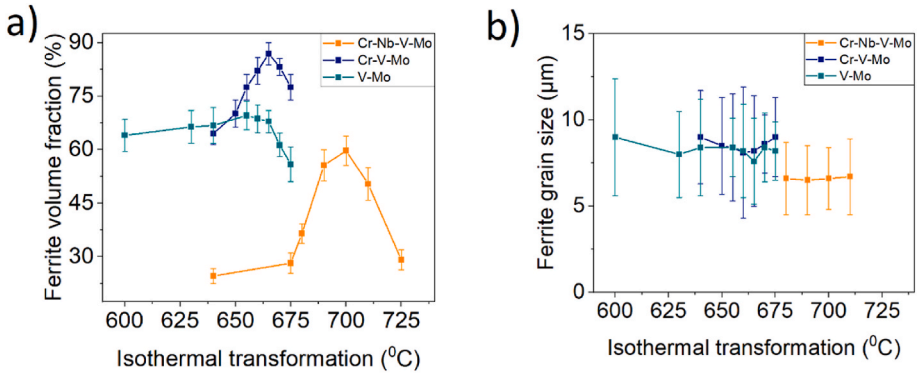

Fig. 6. a) Average ferrite volume fraction and b) Average grain size measured on the optical micrographs from the studied alloys as a function of transformation temperature.

found in all the steels, generally formed through interphase precipitation. An inter-sheet spacing of ~ 70 nm was measured for the V–Mo steel isothermally transformed at 655 °C. The Cr–V–Mo steel, Fig. 9, showed the presence of fine curved IP with row spacing distance of ~ 115 nm. Two precipitate types were identified in the diffraction patterns, namely, VC and V_4C_3. The Cr–Nb–V–Mo steel contained IP, but the precipitates and the inter-row spacing (~150 nm) were larger than in the Nb free steels. This is not surprising given the higher transformation temperatures required in this steel. The orientation relationships were identified from selected area diffraction patterns. It was found that the V_4C_3 precipitates are rod-shaped lying preferentially along two $(011)_\alpha$ directions. The (V,Mo)C and $(V,Mo)_4C_3$ precipitates exhibit the Baker-Nutting orientation relationships with respect to the ferrite matrix. In contrast, the VC exhibits a $[1\ 1\ 1]_{VC}\ 0\ 1\ 1\ ]\ ||]_\alpha$ orientation relationship. This orientation relationship is associated with two possibilities: 1) a semi-coherent Nishiyama-Wassermann orientation relationship, which was observed in relative coarse (∅ >15 nm) interphase precipitation aged for times over 60 min at the transformation temperature, with the precipitate coarsening resulting in a rotation of the precipitate's orientation relationship from the original Baker-Nutting [28,29]. 2) in the Cr–Nb–V–Mo steel, the VC resulted from a mixture of planar and curved interphase precipitation with regular sheet spacing (Fig. 10 a)), indicating the growth of the ferrite is related to the movement of the incoherent α/γ interface at high temperatures [8]. Also, the precipitate size and the interparticle distance increase, which is because of the reduced nucleation rate due to the decreased driving force, and the accelerated carbide growth, because of the increased diffusion rate [8].

The composition, volume fraction and size of the interphase precipitates was determined using extraction replicas in the TEM. An example is given in Fig. 10. The carbon extraction replicas present the same values of size distribution as thin foils within experimental error [10]. In order to obtain the volume fraction of the interphase precipitation (f_V), Equation (1) is commonly used to estimate the f_V of randomly distributed interphase precipitated carbides [30,31] because of its correlation between the number of precipitates observed in a TEM image (n), their average radius of the precipitates ($\overline{R}_v$), the volume of the foil specimen (V), with the average diameter of the precipitates (d), the area percentage of the precipitates in the TEM image (f_s) and the TEM specimen thickness (h) easily obtained from carbon extraction replicas.

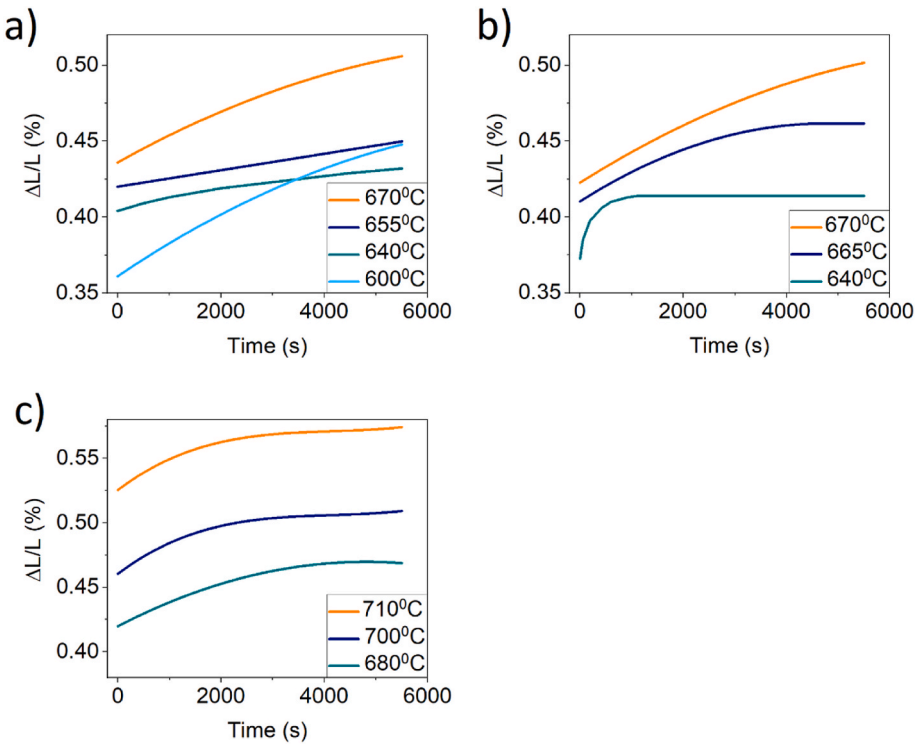

Fig. 7. Dilatation curves of the samples isothermally treated at temperatures between 600 °C and 710 °C. a) V–Mo, b) Cr–V–Mo, c) Cr–Nb–V–Mo.

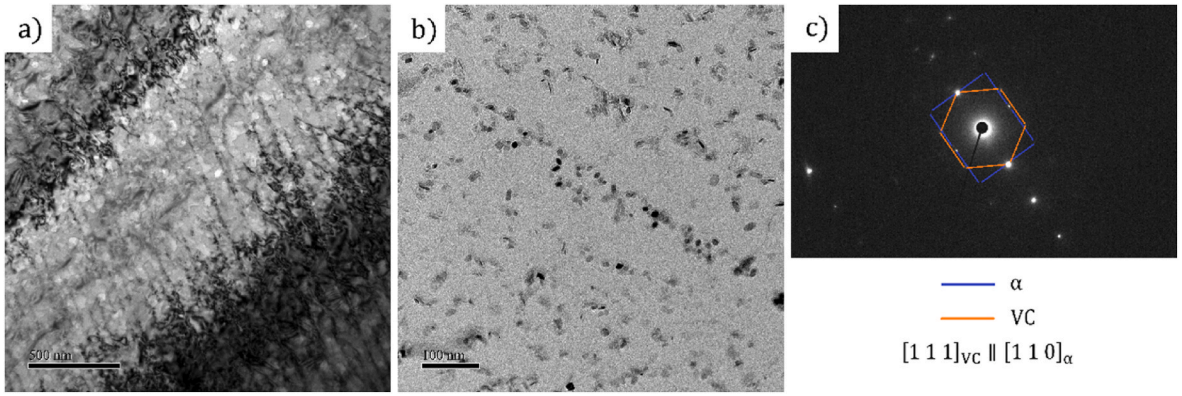

Fig. 8. a) TEM micrographs showing the interphase precipitation in V–Mo steel taken from isothermal treatment at 640 °C for 90min. a) IP distribution in a thin foil sample, b) IP in the V–Mo steel (carbon extraction replica), c) diffraction pattern of the IP in the V–Mo steel.

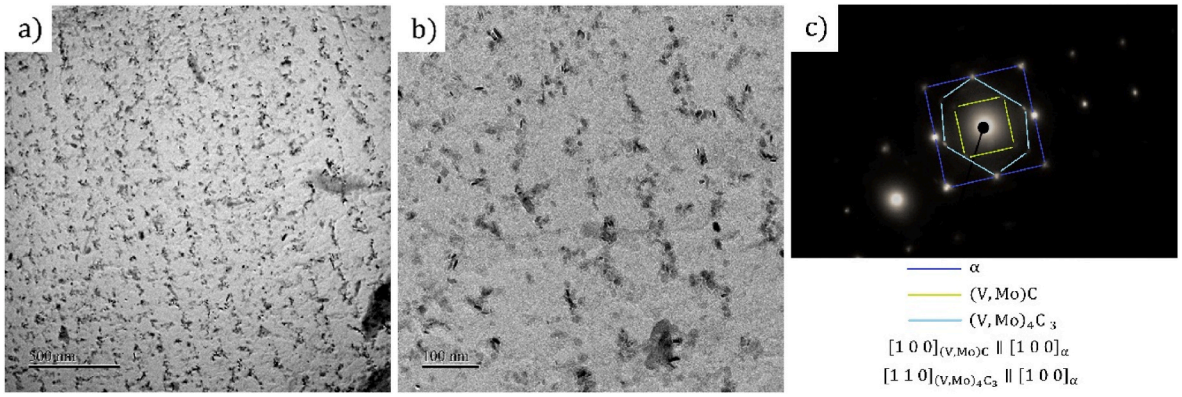

Fig. 9. a) TEM micrographs showing the interphase precipitation in Cr–V–Mo steel taken from isothermal treatment at 660 °C for 90min. a) IP distribution in a thin foil sample, b) IP in the Cr–V–Mo steel (carbon extraction replica), c) diffraction patterns of the IP in the Cr–V–Mo steel.

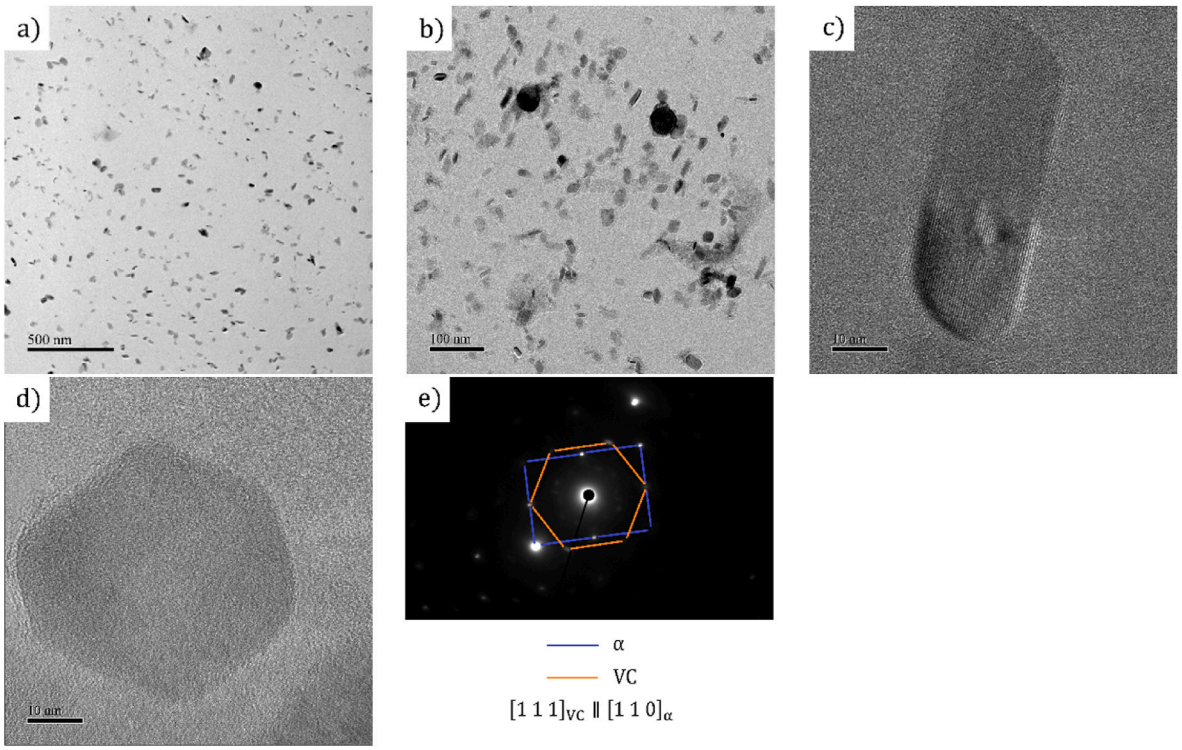

Fig. 10. a) TEM micrographs showing the interphase precipitation in Cr–Nb–V–Mo steel taken from isothermal treatment at 700 °C for 90min. a), b) Precipitate distributions in a carbon extraction replica of the Cr–Nb–V–Mo stee, c) and d) IP precipitation particles observed in a carbon extraction replica, e) diffraction pattern of the IP.

$$f_V = \frac{\frac{4}{3}\pi\left(\frac{d}{2}\right)^3 \bullet n}{V} = \frac{2}{3} d \bullet \frac{f_s}{h} \qquad \text{Equation 1}$$

However, Equation (1) is only applicable to a uniform distribution of precipitates whereas in this case the majority of the precipitates are located in parallel rows, with clear spaces in between. To obtain the f_V, several TEM images from the carbon extraction replicas were obtained and analysed. The TEM images with aligned parallel rows of precipitates were used as this would be the closest to viewing the IP along the $[001]_\alpha$ zone direction, which is the most appropriate imaging orientation and gives a condition where different samples can be compared. Equation (1)

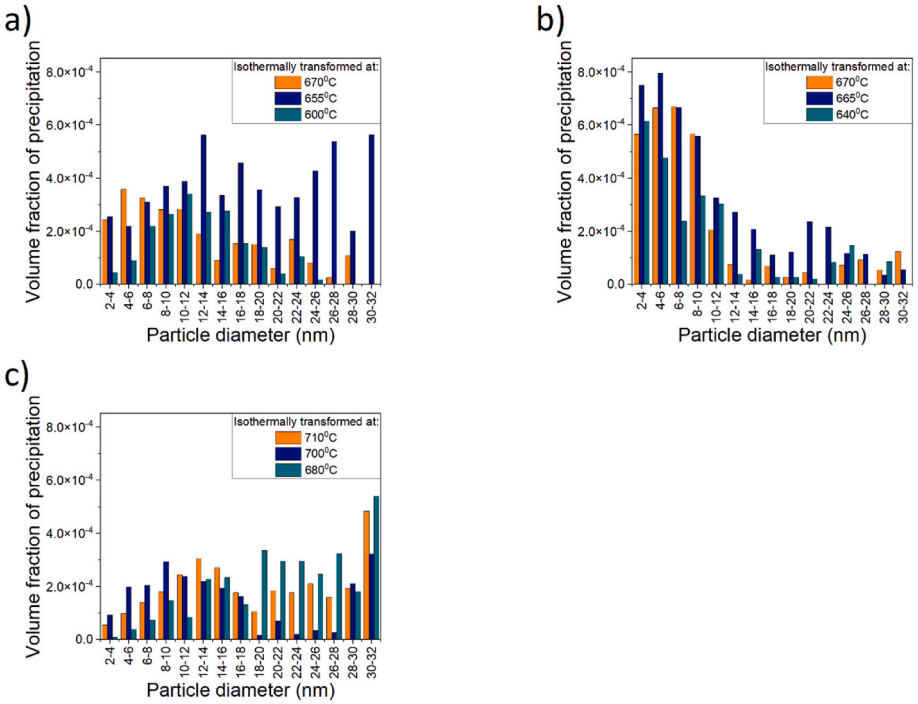

Fig. 11. Size distribution of the IP from the carbon extraction replicas extracted from all the steels studied. a) V–Mo steel, b) Cr–V–Mo steel, c) Cr–Nb–V–Mo steel.

had to be modified to be appropriate to carbon extraction replica samples, which is approximately a two-dimensional sample, rather than a thin foil where the volume can be accurately measured. The volume of the foil specimen (V) in Equation (1) is replaced by the inter-row volume (V_{row}) which is the area observed in the TEM image from the carbon extraction replica ($A_{replica}$) times the IP inter-row distance (L_{rows}). The average volume of the IP is the average projected area of the IP measured on the carbon extraction replicas ($\overline{A}_n$) multiplied by 4 $\bar{r}/3$, where ($\bar{r}$) is the average IP radius. The factor $\overline{A}_n \bullet n$ is the total area of the IP projected on the TEM image, which divided by the total observed area ($A_{replica}$) which results in the percentage of the area occupied by the IP on a carbon extraction replica image (f_s) being:

$$f_V = \frac{\frac{4}{3}\pi\left(\frac{d}{2}\right)^3 \bullet n}{V_{row}} = \frac{\overline{A}_n \bullet \frac{4\bar{r}}{3} \bullet n}{A_{replica} \bullet L_{rows}} = f_s \frac{\frac{4\bar{r}}{3}}{L_{rows}} \quad \text{Equation 2}$$

Figs. 11 and 12 show how the addition of Cr increases the volume fraction of fine IP. In this analysis, particles $\varnothing < 2$ nm were discarded because they were difficult to differentiate from noise. Comparing the V–Mo and Cr–Mo–V, the addition of Cr increases the total volume fraction of precipitates fine enough to contribute to strengthening, but the % of fine precipitates was higher in the V–Mo steel except for temperatures at which the maximum ferrite was reached. The Cr-free steel also exhibited a significant number of relatively large precipitates (15 nm $\leq \varnothing \leq$ 30 nm), but of course the larger particles contribute more significantly to the volume fraction than the finer ones.

IP was not obtained in the Cr–Nb–V–Mo steel at a transformation temperature of 640 °C because a bainitic structure was obtained. At a transformation temperature of 680 °C IP was present, but the size was relatively coarse, Fig. 11 c), giving an overall higher volume fraction of IP compared to 700 °C. As the transformation temperature increased from 680 to 700 °C the proportion of fine IP increased, with similar distributions to the Cr–V–Mo steel transformed at 640–665 °C. This clearly shows the relevance of altering transformation temperature to maximize the IP with $\varnothing < 20$ nm to improve the mechanical properties of microalloyed steels.

3.5. Tensile properties

Fig. 13 a), c) and e) present the engineering strain-stress curves of the three different steels for various transformation temperatures. Fig. 13 b), d) and f) give the mechanical properties obtained from all tensile tests. Comparing the V–Mo and the Cr–V–Mo steels, the addition of Cr produces an increase in all of the yield strength, UTS and the total elongation at the maximum values. The maximum values occur at a slightly higher transformation temperature in the Cr–V–Mo steel compared to the V–Mo steel by about 5–10 °C, although the peak temperature was different for yield strength and UTS.

For the Cr–Nb–V–Mo steel, isothermal transformation at 640 °C produces a bainitic microstructure that provides a much higher yield and ultimate tensile strength with a relatively high value of total elongation, but with a very reduced homogeneous elongation, Fig. 13e). Clearly, this microstructure should not be compared to the DP steels studied here. As the transformation temperature increased the yield strength and UTS decreased to a minimum around 700 °C but then increased up to maximum values at 725 °C. The maximum yield strength was marginally higher than the Cr–V–Mo steel, while the maximum tensile strength was similar, but with slightly higher total elongation.

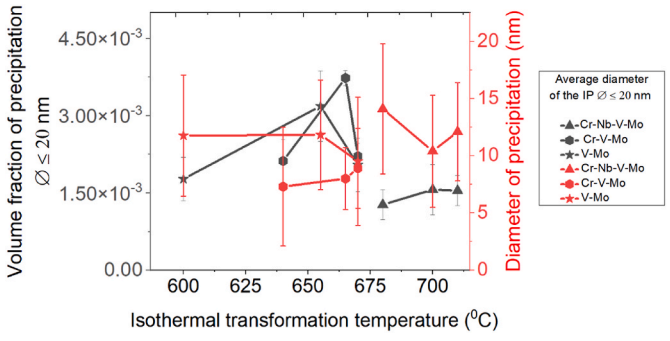

Fig. 12. Average volume fraction and average diameter of the IP found within the ferrite isothermally transformed.

4. Discussion

The products of the isothermal transformation of the V–Mo and Cr–V–Mo steels between 600 °C and 675 °C gave a dual phase structure that was generally polygonal ferrite and martensite, Figs. 3–5. In general, the Cr addition accelerates the transformation kinetics of the microalloyed steels. Moreover, the addition of Cr to the V–Mo steel resulted in a higher volume fraction of ferrite, and therefore less martensite. The maximum volume fraction of ferrite occurred at lower transformation temperature in the V–Mo compared to the Cr–V–Mo steel, indicating a small, but important, change to the TTT diagram through the addition of Cr. Moreover, the addition of Cr also increased the temperature at which the interphase precipitation was maximised compared to the V–Mo steel, discussed below. This is important as comparing the mechanical properties of a steel with and without Cr at the same transformation temperature is likely to be misleading as to the effect of Cr on the microstructure.

All the engineering stress-strain curves presented in Fig. 11 show continuous yielding, low yield ratio, among other characteristics of DP steels. Ferrite yields discontinuously, however, its yielding changes to continuous when used as the matrix in DP steels [32–34], suggesting a gradual and continuous initiation of plastic flow steels [35]. This can be attributed to the stresses produced in the ferrite as a secondary effect of the strains produced by the martensite transformation, in addition to the plastic incompatibility between the constituent phases. These stresses cause ferrite micro yielding around the martensite islands, initiating plastic flow in several ferritic regions throughout the microstructure at lower stress compared with the yield stress of bulk ferrite [36,37]. The presence of harder second phase constituents bring an important contribution to the DP strengths [38]. Moreover, the strength of DP steels mostly increases with decreasing average ferrite grain size (d_f) and increasing the volume fraction of martensite (V_m), with a much more dominant effect of the V_m [39–41].

All three steels contained extensive interphase precipitation in the ferrite (except the Cr–Nb–V–Mo steel transformed at 640 °C, which had a bainitic structure). The nature of the γ→α interface strongly determines the type of interphase precipitation that is produced. It has been shown that a difference in the nucleation sites of interphase-precipitated carbides and the carbide fibers [42], such that fibrous precipitates are favoured by an incoherent interface [43], and a deceleration of the γ→α transformation by alloying elements additions such as Mn [44]. Chen et al. [42,45] suggest that the formation of the carbide fibres is a secondary stage of IP formation, only occurring when a great part of the driving force is consumed by the γ→α transformation. In the current work, planar interphase precipitation was observed at low isothermal transformation temperatures. As the transformation temperature was increased there was a tendency to more curved interphase precipitation and eventually to random distributions.

In the V–Mo steel, the VC precipitates were generally quasi-spherical or ellipsoidal in shape. The addition of Cr changed the precipitate morphology to predominantly rod shaped, along with ellipsoidal shaped precipitates. The Cr addition resulted in a smaller average precipitate size in the Cr–V–Mo compared to the V–Mo steel, but there was not a significant change in the volume fraction of precipitates, which overall provided an increase in precipitation strengthening.

The formation of carbides on the interphase boundary during

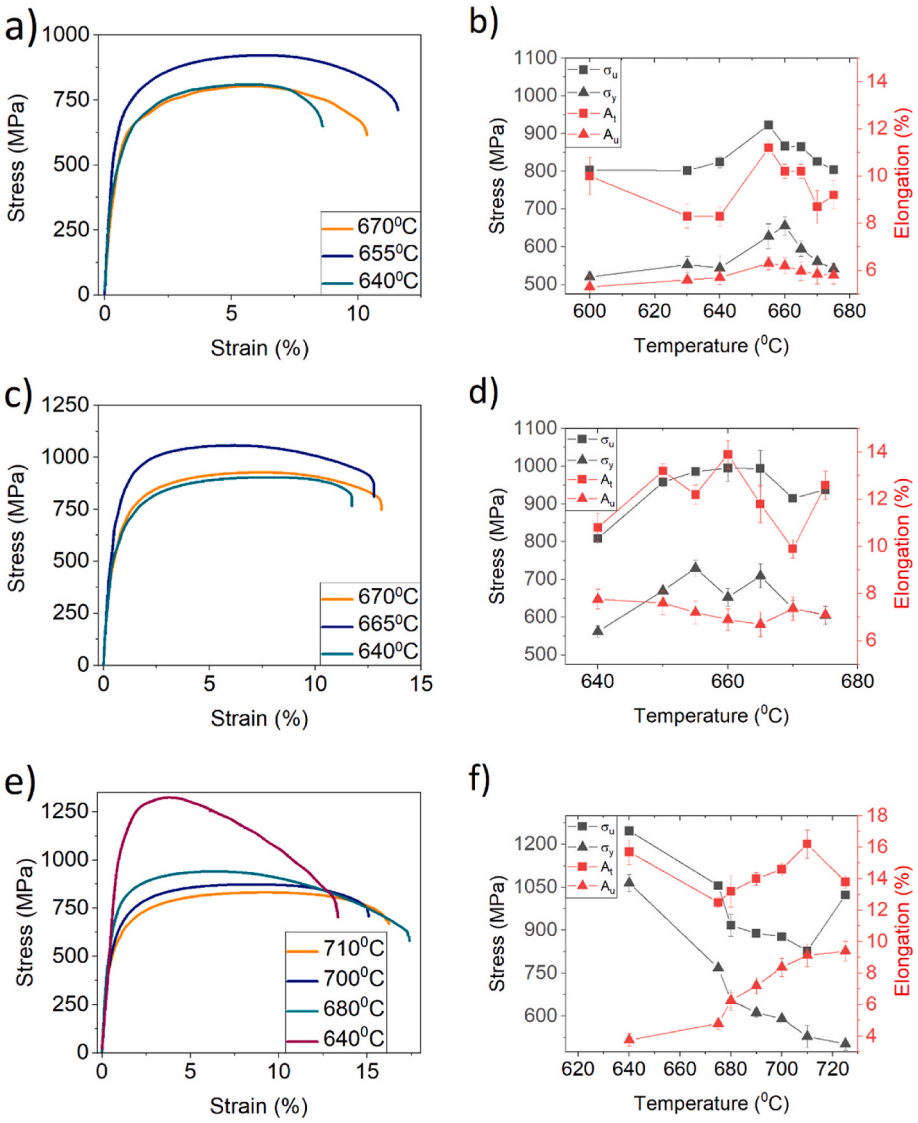

Fig. 13. The strain-stress curves of a) V–Mo steel, c) Cr–V–Mo steel, and e) Cr–Nb–V–Mo steel. Yield strength, ultimate tensile strength and elongation as a function of transformation temperature, b) V–Mo steel, d) Cr–V–Mo steel, and f) Cr–Nb–V–Mo steel. σ_y is the yield strength, σ_u is the ultimate tensile strength, A_t is the total elongation, and A_u is the homogeneous elongation.

transformation is controlled by the driving force for the carbide nucleation and the diffusion of carbide-forming elements along the interface. In the present study, the addition of Cr reduced the average carbide size. There are several possibilities by which Cr can affect the carbide size: through changing the mobility of the γ/α boundary, the chemical free energy of the boundary, the diffusivity along and ahead of the boundary, the interface between the precipitate and the matrix and the structure of the precipitate itself [10]. While the nucleation rate has been calculated for VC and TiC interphase precipitates [10], the values of key variables are missing for the V(Cr,Mo) precipitates observed here, in particularly the effect of Cr on the chemical free energy of the boundary and the diffusivity along and ahead of the boundary are not known. The diffusivity of Cr in Fe is similar to that of Mo in Fe at the isothermal transformation temperatures used here, and therefore it is unlikely that solute diffusivity was the main factor in reducing precipitate size. Therefore, the most probable explanation for the reduction in precipitate size with the addition of Cr is that the Cr increased the interfacial energy of the austenite/ferrite transformation boundary.

To understand the correlation between strength, grain size, and carbide precipitation, the structure-based strength needs to be understood as a function of many other strengthening mechanisms. It can be calculated as follows [37,46]:

$$\Delta\sigma_y = \Delta\sigma_0 + \Delta\sigma_{SS} + \Delta\sigma_{GB} + \Delta\sigma_S + \Delta\sigma_P \quad \text{Equation 3}$$

Where $\Delta\sigma_0$, $\Delta\sigma_{SS}$, $\Delta\sigma_{GB}$, $\Delta\sigma_S$, and $\Delta\sigma_P$ are respectively the lattice friction stress, the solid solute strengthening, the grain boundary strengthening, the dislocation strengthening, and the precipitation strengthening. The Peierls-Nabarro lattice friction stress ($\Delta\sigma_0$) is given by Ref. [47]:

$$\sigma_0 = (2G/1-\nu)\ exp\ (-2\pi w/b) \quad \text{Equation 4}$$

Where G, ν, w, and b are the shear modulus, the Poisson's ratio, the dislocation width and the Burger's vector respectively. The width of edge dislocation is similar among AHSS and microalloyed steels, the reason why several authors [46,48] used 48 MPa as lattice friction stress in their calculations.

The solid solution hardening for ferrite ($\Delta\sigma_{SS}$) [49]:

$$\Delta\sigma_{SS} = 4570[C] + 4570[N] + 37[Mn] + 83[Si] + 470[P] + 38[Cu] + 80[Ti] + 0[Ni] - 30[Cr] \quad \text{Equation 5}$$

The elemental composition is input as the weight percentage of it within the ferrite, which are mainly the same as listed in Table 1 except for the carbon which is the carbon concentration within the ferrite CF, estimated as 0.02 wt%.

The grain refinement strengthening ($\Delta\sigma_{GB}$) (the Hall-Petch relationship [15]) is:

$$\Delta\sigma_{GB} = K_y d_F^{-0.5} \quad \text{Equation 6}$$

K_y is the constant (0.55 MPa $m^{0.5}$ for HSLA steel [15]) and d_F is the average grain size measured in m.

The increased yield stress produced by the increased dislocation density is [50]:

$$\Delta\sigma_S = \alpha M G b\sqrt{\rho} \quad \text{Equation 7}$$

Where α is a material constant (0.33 used for DP steels [37]), M is the Taylor factor (2.75 for ferrite), G is the shear modulus (80.3 GPa), b is the Burgers vector (2.48×10^{-10} m), ρ is the dislocation density (estimated to be 5×10^{13} m^{-2} for the ferrite matrix during isothermal transformation [10]).

The contribution of precipitation to the yield strength of microalloyed steels can be calculated using the Ashby-Orowan model [45,51,52]:

$$\Delta\sigma_P = 8995 * \frac{f_V^{1/2}}{d} ln(2.417d) \quad \text{Equation 8}$$

f_V and d are the volume fraction of the interphase precipitation, and the average diameter of precipitation in nanometers respectively. These calculations have been done with the values obtained from precipitates $\varnothing < 20$ nm which is the maximum size at which precipitates contribute to strength.

The different microstructural contributions to the yield strength of the different steels are plotted in Fig. 14, assuming a linear addition as presented in Equation (3). The addition of chromium clearly increases the IP contribution, which is the second largest individual contributor for V–Mo and the largest for Cr–V–Mo microalloyed steels. Although, the addition of Cr plus Nb increases the grain refinement strengthening, this is at the expense of the IP precipitation hardening. This is clearly demonstrated in the radar chart in Fig. 15 which shows how the Cr addition increases the yield strength and increases the homogeneous elongation through an increase in isothermally transformed ferrite, and also from the increased fine IP ($\varnothing < 20$ nm) volume fraction. Note that the addition of Cr + Nb at isothermal transformation temperatures below 700 °C gave relatively large precipitates, which strongly affects the volume fraction, but the combination of microstructural features, particularly solid solution hardening and grain boundary strengthening gave a good combination of ultimate strength, homogeneous and total elongation plus a good yield strength.

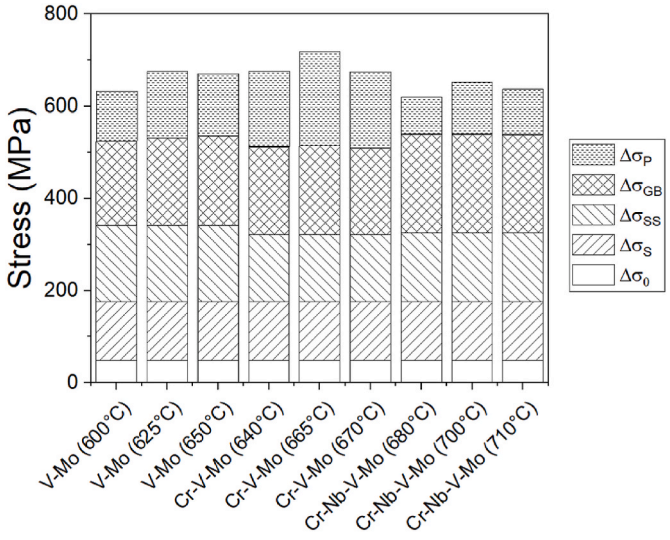

Fig. 14. Yield strength individual contributors of microalloyed steels as a function of the isothermal transformation temperature.

This expression of the yield strength as a direct sum of the different contributors gives errors of more than 100 MPa in all the steels, compared with the experimental results. Other researches [53,54] included values dependant of the volume fraction and the carbon content of the martensite to the calculation of the tensile properties. Kang et al. [48] presented a modified root-mean-square model (Equation (9)) to predict in good agreement the yield strength of DP (α+M) steels.

$$\Delta\sigma_y = \left[(\sigma_0)^2 + (\sigma_{SS})^2 + (\sigma_{GB})^2 + (\sigma_S)^2\right]^{1/2} - 8\left(V_M/V_F\right)^2 \quad \text{Equation 9}$$

The Kang et al. model does not include the effect of the precipitation hardening ($\Delta\sigma_P$). This is included in other models (such as Equation (3)) but these do not consider any contribution of the martensite to the yield strength. To address these shortcomings, we present a modified model expressed in Equation (10) which match with the yield strength obtained from the tensile tests. The major contribution from IP to the global strengthening comes from the ferrite, for that reason the contribution of precipitation in the martensite can be neglected. The constant k for all the alloys studied in this investigation is 1.9, providing results that match with all the experiments performed for this study within a maximum margin of ±50 MPa (except for the microstructures with bainite), but in most cases the difference is less than ±25 MPa. Thus, the shortfall in strength prediction from equation (3) arose from the contribution from the martensite.

$$\Delta\sigma_y = k \bullet \left[\left[(\sigma_0)^2 + (\sigma_{SS})^2 + (\sigma_{GB})^2 + (\sigma_S)^2 + (\sigma_P)^2\right]^{1/2} - 8\left(V_M/V_F\right)^2\right] \quad \text{Equation 10}$$

5. Conclusions

The addition of Cr and its effects on the interphase precipitation and therefore on the mechanical properties of a V–Mo dual-phase (DP) microalloyed steel was evaluated. The following conclusions can be made:

1. Isothermal transformation of the V–Mo and Cr–V–Mo steels between 600 °C and 675 °C gave a dual phase structure that was generally polygonal ferrite and martensite. The Cr addition accelerated the kinetics of transformation to ferrite and resulted in a higher volume fraction of ferrite, and therefore less martensite.
2. All three steels contained extensive interphase precipitation in the ferrite (except the Cr–Nb–V–Mo steel transformed at 640 °C, which had a bainitic structure). The addition of Cr increased the temperature at which the interphase precipitation was maximised compared to the V–Mo steel. Therefore, comparing the mechanical properties of a steel with and without Cr at the same transformation temperature is likely to be misleading as to the effect of Cr on the microstructure.
3. The Cr addition resulted in a smaller average precipitate size in the Cr–V–Mo compared to the V–Mo steel, but there was not a significant change in the volume fraction of precipitates. The result was an increase in precipitation strengthening.
4. The optimum tensile properties in the Cr–V–Mo steel were obtained at 10 °C higher isothermal transformation temperature than in V–Mo steel, which gave a higher volume fraction of transformed ferrite, and the smallest interphase precipitate size.
5. The addition of Cr + Nb at isothermal transformation temperatures below 700 °C gave relatively large interphase precipitates, which reduced precipitation hardening, but this was offset by the grain size

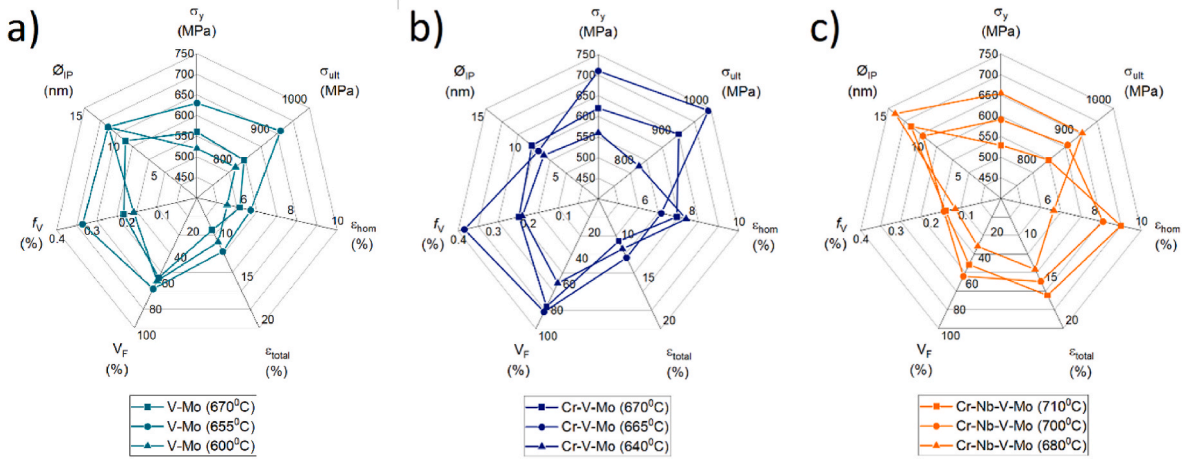

Fig. 15. Radar chart correlating the tensile properties for microalloyed applications with the ferrite volume fraction, and the IP volume fraction and diameter of a) V–Mo, b) Cr–V–Mo, and c) Cr–Nb–V–Mo microalloyed steels.

reduction which resulted in a good combination of yield strength, ultimate strength and both homogeneous and total elongation.

6. A modification to the calculation of the IP volume fraction of microalloyed steels from extraction replica samples is presented, which provides the correct input to the Ashby-Orowan model for calculating the precipitation hardening effect.
7. A modification was made to the root-mean-square model by Kang et al. [48] to calculate the yield strength of dual phase (α+M) microalloyed steels. Excellent agreement was found between calculation and experiment, allowing the individual components of precipitation strengthening, ferrite fraction and grain size, and martensite proportion to be identified. Thereby, the optimum composition and process conditions are identified.

CRediT authorship contribution statement

Karol F. Rodriguez-Galeano: Data curation, Formal analysis, Investigation, Writing – original draft. **John Nutter:** Investigation, Writing – review & editing. **Yunus Azakli:** Investigation. **Carl Slater:** Investigation. **W. Mark Rainforth:** Conceptualization, Funding acquisition, Writing – review & editing.

Declaration of competing interest

The authors declare that they have no known competing financial interests or personal relationships that could have appeared to influence the work reported in this paper.

Data availability

Data will be made available on request.

Acknowledgements

The authors are grateful to the Neville and Eileen Baker Charitable Trust for the scholarship for Karol F. Rodriguez-Galeano. The authors also wish to acknowledge the Henry Royce Institute for Advanced Materials, funded through EPSRC grants EP/R00661X/1, EP/S019367/1 for access to the JEOL JEM-F200 through Royce@Sheffield.

References

[1] T. Baudin, C. Quesne, J. Jura, R. Penelle, Microstructural characterization in a hot-rolled, two-phase steel, Mater. Char. 47 (5) (2001) 365–373, https://doi.org/10.1016/S1044-5803(02)00183-3.
[2] N. Terao, B. Cauwe, Influence of additional elements (Mo, Nb, Ta and B) on the mechanical properties of high-manganese dual-phase steels, J. Mater. Sci. 23 (5) (1988) 1769–1778, https://doi.org/10.1007/BF01115721.
[3] P. Tsipouridis, E. Werner, C. Krempaszky, E. Tragl, Formability of high strength DP steels, Steel Res. Int. 77 (9) (2006) 654–667. file://ce/rd_organisation/PTA-MAD/Common/10 Literature/2008/AHSS/DP/Tsipouridis (2006) # Formability of high strength DP steels.pdf.
[4] A.T. Davenport, L.C. Brossard, R.E. Miner, Precipitation in microalloyed high-strength low-alloy steels, J. Miner. Met. Mater. Soc. 27 (6) (1975) 21–27, https://doi.org/10.1007/BF03355951.
[5] S. Freeman, R.W.K. Honeycombe, Strengthening of titanium steels by carbide precipitation, Met. Sci. 11 (2) (1977) 59–64, https://doi.org/10.1179/msc.1977.11.2.59.
[6] N.K. Balliger, R.W.K. Honeycombe, Coarsening of vanadium carbide, carbonitride, and nitride in low-alloy steels, Met. Sci. 14 (4) (1980) 121–133, https://doi.org/10.1179/030634580790426337.
[7] T. Sakuma, R.W.K. Honeycombe, Microstructures of isothermally transformed Fe-Nb-C alloys, Met. Sci. 18 (9) (1984) 449–454, https://doi.org/10.1179/030634584790419791.
[8] H.W. Yen, P.Y. Chen, C.Y. Huang, J.R. Yang, Interphase precipitation of nanometer-sized carbides in a titanium-molybdenum-bearing low-carbon steel, Acta Mater. 59 (16) (2011) 6264–6274, https://doi.org/10.1016/j.actamat.2011.06.037.
[9] J.H. Jang, Y.U. Heo, C.H. Lee, H.K.D.H. Bhadeshia, D.W. Suh, Interphase precipitation in Ti-Nb and Ti-Nb-Mo bearing steel, Mater. Sci. Technol. 29 (3) (2013) 309–313, https://doi.org/10.1179/1743284712Y.0000000131.
[10] P. Gong, X.G. Liu, A. Rijkenberg, W.M. Rainforth, The effect of molybdenum on interphase precipitation and microstructures in microalloyed steels containing titanium and vanadium, Acta Mater. 161 (2018) 374–387, https://doi.org/10.1016/j.actamat.2018.09.008.
[11] V.B. Ginzburg, Steel-Rolling Technology: Theory and Practice, CRC Press, 1989.
[12] A.T. Davenport, F.G. Berry, R.W.K. Honeycombe, F.G. Berry, R.W.K. Honeycombe, Interphase precipitation in iron alloys interphase precipitation in iron alloys, Sci. J. 2 (1968) 104–106, https://doi.org/10.1179/030634568790443341, 1(1968).
[13] A.T. Davenport, R.W.K. Honeycombe, Precipitation of carbides at γ -α boundaries in alloy steels, Proc R Soc Lond A Math Phys Sci 322 (1549) (1971) 191–205.
[14] R.W.K. Honeycombe, Fundamental aspects of precipitation in microalloyed steels, HSLA Steels: Metallurgy and Applications (1985) 243–250.
[15] Y. Funakawa, T. Shiozaki, K. Tomita, T. Yamamoto, E. Maeda, Development of high strength hot-rolled sheet steel consisting of ferrite and nanometer-sized carbides, ISIJ Int. 44 (11) (2004) 1945–1951, https://doi.org/10.2355/isijinternational.44.1945.
[16] Y.J. Zhang, G. Miyamoto, K. Shinbo, T. Furuhara, Effects of α/γ orientation relationship on VC interphase precipitation in low-carbon steels, Scripta Mater. 69 (1) (2013) 17–20, https://doi.org/10.1016/j.scriptamat.2013.03.020.
[17] S.P. Tsai, T.C. Su, J.R. Yang, C.Y. Chen, Y.T. Wang, C.Y. Huang, Effect of Cr and Al additions on the development of interphase-precipitated carbides strengthened dual-phase Ti-bearing steels, Mater. Des. 119 (2017) 319–325, https://doi.org/10.1016/j.matdes.2017.01.071.
[18] N.A. Gorokhova, V.I. Sarrak, S.O. Suvorava, Solubility of titanium and niobium carbides in high-chromium ferrite, Met Sci Heat Treat Met(Engl Transl);(United States). 28 (4) (1986).
[19] A. Ray, Niobium microalloying in rail steels, Mater. Sci. Technol. 33 (14) (2017) 1584–1600, https://doi.org/10.1080/02670836.2017.1309111.
[20] S. Koyama, T. Ishii, K. Narita, Effects of Mn, Si, Cr, and Ni on the Solution and Precipitation of Niobium Carbide in Iron Austenite, Kobe Steel Ltd, Japan, 1971.
[21] J.F. Da Silva Filho, C.A.S. De Oliveira, N. Fonstein, et al., Effect of Cr additions on ferrite recrystallization and austenite formation in dual-phase steels heat treated in

the intercritical temperature range, Mater. Res. 19 (1) (2016) 258–266, https://doi.org/10.1590/1980-5373-MR-2015-0641.
[22] E.J. Palmiere, C.I. Garcia, A.J. De Ardo, Compositional and microstructural changes which attend reheating and grain coarsening in steels containing niobium, Metall. Mater. Trans. A 25 (2) (1994) 277–286, https://doi.org/10.1007/BF02647973.
[23] K.F. Rodriguez-Galeano, L.F. Romano-Acosta, E.J. Palmiere, W.M. Rainforth, A new approach to etching low-carbon microalloyed steels to reveal prior austenite grain boundaries and the dual-phase microstructure, J. Microsc. 289 (2) (2023) 73–79, https://doi.org/10.1111/jmi.13153.
[24] H.S. Yang, H.K.D.H. Bhadeshia, Austenite grain size and the martensite-start temperature, Scripta Mater. 60 (7) (2009) 493–495, https://doi.org/10.1016/j.scriptamat.2008.11.043.
[25] A. Ghatei Kalashami, A. Kermanpur, E. Ghassemali, A. Najafizadeh, Y. Mazaheri, Correlation of microstructure and strain hardening behavior in the ultrafine-grained Nb-bearing dual phase steels, Mater. Sci. Eng., A 678 (September) (2016) 215–226, https://doi.org/10.1016/j.msea.2016.09.108.
[26] R. Song, N. Fonstein, H.J. Jun, N. Pottore, D. Bhattacharya, S. Jansto, Effects of Nb on microstructural evolution and mechanical properties of low-carbon cold-rolled dual-phase steels, Metallogr Microstruct Anal 3 (3) (2014) 174–184, https://doi.org/10.1007/s13632-014-0133-9.
[27] A. Ghatei Kalashami, A. Kermanpur, A. Najafizadeh, Y. Mazaheri, Effect of Nb on microstructures and mechanical properties of an ultrafine-grained dual phase steel, J. Mater. Eng. Perform. 24 (8) (2015) 3008–3017, https://doi.org/10.1007/s11665-015-1539-5.
[28] H.W. Yen, C.Y. Chen, T.Y. Wang, C.Y. Huang, J.R. Yang, Orientation relationship transition of nanometre sized interphase precipitated TiC carbides in Ti bearing steel, Mater. Sci. Technol. 26 (4) (2010) 421–430, https://doi.org/10.1179/026708309X12512744154207.
[29] N.C. Law, S.A. Parsons, P.R. Howell, D.V. Edmonds, Crystallography of carbide precipitation at transformation interfaces during austenite decomposition in a low-alloy steel, Mater. Sci. Technol. 3 (8) (1987) 642–648, https://doi.org/10.1179/mst.1987.3.8.642.
[30] X.L. Li, C.-S. Lei, -T. Deng, Y.-M. Li, Y. Tian, Z.-D. Wang, G.D. Wang, Carbide precipitation in ferrite in Nb-V-bearing low-carbon steel during isothermal quenching process, Acta Metall Sin (English Lett. 30 (11) (2017) 1067–1079, https://doi.org/10.1007/s40195-017-0632-1.
[31] J. Cong, J. Li, J. Fan, P. Liu, R.D.K. Misra, C. Shang, X. Wang, The impact of interphase precipitation on the mechanical behavior of fire-resistant steels at an elevated temperature, Materials 13 (19) (2020) 1–13, https://doi.org/10.3390/ma13194294.
[32] M. Calcagnotto, D. Ponge, D. Raabe, Ultrafine grained ferrite/martensite dual phase steel fabricated by large strain warm deformation and subsequent intercritical annealing, ISIJ Int. 48 (8) (2008) 1096–1101, https://doi.org/10.2355/isijinternational.48.1096.
[33] K.T. Park, S.Y. Han, B.D. Ahn, D.H. Shin, Y.K. Lee, K.K. Um, Ultrafine grained dual phase steel fabricated by equal channel angular pressing and subsequent intercritical annealing, Scripta Mater. 51 (9) (2004) 909–913, https://doi.org/10.1016/j.scriptamat.2004.06.017.
[34] Y Il Son, Y.K. Lee, K.T. Park, C.S. Lee, D.H. Shin, Ultrafine grained ferrite-martensite dual phase steels fabricated via equal channel angular pressing: microstructure and tensile properties, Acta Mater. 53 (11) (2005) 3125–3134, https://doi.org/10.1016/j.actamat.2005.02.015.
[35] T. Sakaki, K. Sugimoto, T. Fukuzato, Role of internal stress for continuous yielding of dual-phase steels, Acta Metall. 31 (10) (1983) 1737–1746, https://doi.org/10.1016/0001-6160(83)90172-4.
[36] M.A. Maleque, Y.M. Poon, H.H. Masjuki, The effect of intercritical heat treatment on the mechanical properties of AISI 3115 steel, J. Mater. Process. Technol. 153–154 (1–3) (2004) 482–487, https://doi.org/10.1016/j.jmatprotec.2004.04.391.
[37] Y. Mazaheri, A. Kermanpur, A. Najafizadeh, Strengthening mechanisms of ultrafine grained dual phase steels developed by new thermomechanical processing, ISIJ Int. 55 (1) (2015) 218–226, https://doi.org/10.2355/isijinternational.55.218.
[38] A. Kumar, S.B. Singh, K.K. Ray, Influence of bainite/martensite-content on the tensile properties of low carbon dual-phase steels, Mater. Sci. Eng., A 474 (1–2) (2008) 270–282, https://doi.org/10.1016/j.msea.2007.05.007.
[39] M. Mazinani, W.J. Poole, Effect of martensite plasticity on the deformation behavior of a low-carbon dual-phase steel, Metall Mater Trans A Phys Metall Mater Sci 38 (2) (2007) 328–339, https://doi.org/10.1007/s11661-006-9023-3.
[40] C. Peng-Heng, A.G. Preban, The effect of ferrite grain size and martensite volume fraction on the tensile properties of dual phase steel, Acta Metall. 33 (5) (1985) 897–903, https://doi.org/10.1016/0001-6160(85)90114-2.
[41] R.G. Davies, Influence of martensite composition and content on the properties of dual phase steels, Metall. Trans. A 9 (5) (1978) 671–679, https://doi.org/10.1007/BF02659924.
[42] M.Y. Chen, H.W. Yen, J.R. Yang, The transition from interphase-precipitated carbides to fibrous carbides in a vanadium-containing medium-carbon steel, Scripta Mater. 68 (11) (2013) 829–832, https://doi.org/10.1016/j.scriptamat.2013.01.020.
[43] D.V. Edmonds, Occurrence of fibrous VC during transformation of an Fe-V-C steel, J Iron Steel Inst 210 (5) (1972) 363–365.
[44] F.a. Khalid, D.V. Edmonds, Interphase precipitation in microalloyed engineering steels and model alloy, Mater. Sci. Technol. 9 (5) (1993) 384–396, https://doi.org/10.1179/026708393790350468.
[45] M.Y. Chen, M. Gouné, M. Verdier, Y. Bréchet, J.R. Yang, Interphase precipitation in vanadium-alloyed steels: strengthening contribution and morphological variability with austenite to ferrite transformation, Acta Mater. 64 (2014) 78–92, https://doi.org/10.1016/j.actamat.2013.11.025.
[46] X. Mao, X. Huo, X. Sun, Y. Chai, Strengthening mechanisms of a new 700 MPa hot rolled Ti-microalloyed steel produced by compact strip production, J. Mater. Process. Technol. 210 (12) (2010) 1660–1666, https://doi.org/10.1016/j.jmatprotec.2010.05.018.
[47] W. Soboyejo, Mechanical Properties of Engineered Materials, CRC press, 2002.
[48] Y.L. Kang, Q.H. Han, X.M. Zhao, M.H. Cai, Influence of nanoparticle reinforcements on the strengthening mechanisms of an ultrafine-grained dual phase steel containing titanium, Mater. Des. 44 (2013) 331–339, https://doi.org/10.1016/j.matdes.2012.07.068.
[49] Q.L. Yong, M.T. Ma, B.R. Wu, Microalloyed Steel-Physical and Mechanical Metallurgy, Beijing Mech Eng Press, 1989.
[50] N. Kamikawa, Y. Abe, G. Miyamoto, Y. Funakawa, T. Furuhara, Tensile behavior of Ti, Mo-added low carbon steels with interphase precipitation, ISIJ Int. 54 (1) (2014) 212–221, https://doi.org/10.2355/isijinternational.54.474.
[51] H.J. Kestenbach, S.S. Campos, E.V. Morales, Role of interphase precipitation in microalloyed hot strip steels, Mater. Sci. Technol. 22 (6) (2006) 615–626, https://doi.org/10.1179/026708306X81487.
[52] S.C. Krishna, N.K. Gangwar, A.K. Jha, B. Pant, On the prediction of strength from hardness for copper alloys, J. Mater. 2013 (2013) 1–6, https://doi.org/10.1155/2013/352578.
[53] M. Calcagnotto, Y. Adachi, D. Ponge, D. Raabe, Deformation and fracture mechanisms in fine- and ultrafine-grained ferrite/martensite dual-phase steels and the effect of aging, Acta Mater. 59 (2) (2011) 658–670, https://doi.org/10.1016/j.actamat.2010.10.002.
[54] P. Movahed, S. Kolahgar, S.P.H. Marashi, M. Pouranvari, N. Parvin, The effect of intercritical heat treatment temperature on the tensile properties and work hardening behavior of ferrite-martensite dual phase steel sheets, Mater. Sci. Eng., A 518 (1–2) (2009) 1–6, https://doi.org/10.1016/j.msea.2009.05.046.